HHS Public Access

Author manuscript

Angiogenesis. Author manuscript; available in PMC 2018 November 01.

Published in final edited form as:

Angiogenesis. 2017 November ; 20(4): 581–598. doi:10.1007/s10456-017-9572-7.

Prox1-GFP/Flt1-DsRed Transgenic Mice: An Animal Model for Simultaneous Live Imaging of Angiogenesis and Lymphangiogenesis

Wei Zhong, MD[1,2,3], **Xinbo Gao, MD, PhD**[1], **Shuangyong Wang, MD, PhD**[1], **Kyuyeon Han, PhD**[1], **Masatsugu Ema, PhD**[4], **Susanne Adams**[5], **Ralf H. Adams, PhD**[5], **Mark I. Rosenblatt, MD, PhD, MBA**[1], **Jin-Hong Chang, PhD**[1,*], and **Dimitri T. Azar, MD, MBA**[1,*]

[1]Department of Ophthalmology and Visual Sciences, Illinois Eye and Ear Infirmary, College of medicine, University of Illinois at Chicago, Chicago, Illinois

[2]Department of Ophthalmology, China-Japan Union Hospital, Jilin University, Changchun, Jilin 130033, P.R. China

[3]School of Life Sciences, Jilin University, Changchun, People's Republic of China

[4]Department of Stem Cells and Human Disease Models, Shiga University of Medical Science, Seta, Tsukinowa-cho, Otsu, Shiga, Japan

[5]Faculty of Medicine, Department of Tissue Morphogenesis, Max-Planck-Institute for Molecular Biomedicine and University of Münster, D-48149 Münster, Germany

Abstract

The roles of angiogenesis in development, health, and disease have been studied extensively; however, the studies related to lymphatic system are limited due to the difficulty in observing colorless lymphatic vessels. But recently, with the improved technique, the relative importance of the lymphatic system is just being revealed. We bred transgenic mice in which lymphatic endothelial cells express GFP (Prox1-GFP) with mice in which vascular endothelial cells express DsRed (Flt1-DsRed) to generate Prox1-GFP/Flt1-DsRed (PGFD) mice. The inherent fluorescence of blood and lymphatic vessels allows for direct visualization of blood and lymphatic vessels in various organs via confocal and two-photon microscopy and the formation, branching, and regression of both vessel types in the same live mouse cornea throughout an experimental time course. PGFD mice were bred with CDh5CreERT2 and VEGFR2lox knockout mice to examine specific knockouts. These studies showed a novel role for vascular endothelial cell VEGFR2 in regulating VEGFC-induced corneal lymphangiogenesis. Conditional deletion of vascular endothelial VEGFR2 abolished VEGFA- and VEGFC-induced corneal lymphangiogenesis. These

Address correspondence to: Dimitri T. Azar, MD, MBA (dazar@uic.edu) and Jin-Hong Chang, PhD (changr@uic.edu). Department of Ophthalmology and Visual Sciences, University of Illinois at Chicago, Chicago, IL 60612, Tel (312) 413-5590, Fax: 312-996-7770.

CONFLICTS OF INTEREST The authors declare that they have no competing financial interests

AUTHOR CONTRIBUTIONS Wei Zhong, Xinbo Gao, and Shuangyong Wang performed experiments and data analyses. Susanne Adams and Ralf Adams provide CDh5CreERT2 mice and technical support. Masatsugu Ema provided the Flt1-DsRed mice. Kyuyeon Han, Mark I. Rosenblatt, Jin-Hong Chang, and Dimitri T. Azar planned the research, discussed the data analysis, and wrote the manuscript.

results demonstrate the potential use of the PGFD mouse as a powerful animal model for studying angiogenesis and lymphangiogenesis.

Keywords

Angiogenesis; Lymphangiogenesis; Animal model; In vivo imaging

Blood and lymphatic vessels constitute the complete circulatory system[1]. They do not only play a physiological role in the maintenance of homeostasis during normal development, but are also involved in the development of pathological conditions during ischemia injury, inflammation, and cancer metastasis[2]. Blood vessels carry oxygenated, nutrient-rich blood throughout the body and also recycle deoxygenated blood and wastes [1,3]. Similarly, lymphatic vessels play a vital role in immune surveillance by delivering dendritic cells, macrophages, and neutrophils to lymph nodes and recycling lipids, liquids, and proteins from peripheral tissues back to the circulation system[1]. Recently, researchers have developed several lymphatic or blood vasculature-specific, promoter-driven, fluorescence-reported transgenic mice [4,5]. The transgenic fluorescence of the lymphatic or blood vasculature in Prox1-GFP [6], VEGFR3-YFP [7], Prox1-tdtomato, Flk1-mcherry[8], Flk1-GFP, and Flt1-DsRed mice is valuable because it makes it possible to characterize lymphatic or blood vessel formation in live imaging throughout the experimental time course [6] [8–10]. As an example, Prox1-tdtomato mice have been used to explore the anatomical organization of lymphatic vessels in the brain [11], and Flt1-DsRed mice have been used to investigate the processes underlying blood and nerve guidance [5].

While studies of the distinct processes of hemangiogenesis (HA) and lymphangiogenesis (LA) are valuable for revealing the underlying molecular mechanisms of each, to understand how a treatment targeting one process is likely to affect the other, it will be important to first understand the interdependence of these vascularization processes. Therefore, we sought to generate a mouse model in which both HA and LA can be visualized simultaneously *in vivo*. To create such a model, we bred Prox1-GFP mice, in which lymphatic vessels transgenic express green fluorescence, with Flt1-DsRed mice, in which blood vessels transgenic express red fluorescence, to generate Prox1-GFP/Flt1-DsRed (PGFD) dual-fluorescence reporter mice. Here we demonstrate by confocal and two-photon microscopic imaging that prominent GFP and DsRed signals from lymphatic and blood vessels, respectively, can be observed throughout the mouse body, including in the lung, stomach, skin, heart, intestine, mesentery, and kidney. Moreover, we present how HA and LA can be imaged within the corneas of live mice in response to injury or growth factor pellet implantation as well as how PGFD mice can be bred with other transgenic/knockout mice (i.e. CDh5CreERT2 and VEGFR2lox knockout mice) for experiments to unravel the molecular mechanisms responsible for both forms of neovascularization.

Overall, the PGFD mouse model represents a useful model and valuable experimental resource for studying HA and LA in concert via simultaneous *in vivo* imaging of these processes.

Methods

Animals

Both male and female mouse pups were used for organ imaging. In addition, we used both male and female mice (6–8 weeks old) for injury-induced corneal HA and LA. All procedures/methods were performed as per the US National Institutes of Health Guide for the Care and Use of Laboratory Animals and the ARVO statement for the use of animals in ophthalmic and vision research. The Institutional Animal Care and Use Committees of University of Illinois at Chicago approved the study's experimental protocols. Because surgical procedures on the mouse eye cause traumatic pain, only one eye (the left eye) was operated on in each mouse during the course of the experiment. Surgical operations were performed after the full anesthetization of the animals.

Generation of conditional knockout PGFD mouse model

Floxed *VEGFR2* mice (flk1$^{fl/fl}$) were obtained from Dr. Thomas N. Sato, Nara Institute of Science and Technology. Flk1$^{fl/fl}$ mice were crossed with *Tg(Cdh5-cre/ERT2)1Rha* and PGFD mice to specifically delete exon 3 of VEGFR2. Genotyping of the VEGFR2 wild-type and mutant allele, *Cdh5CreERT2* allele and PGFD was carried out by PCR.

To induce VEGFR2 deletion in adult mice, they were given an intraperitoneal (IP) injection of 80 mg *tamoxifen*/kg (Sigma-Aldrich, T5648, St. Louis, MO) in 200 μl corn oil/5% ethanol for 5 days. Mice were housed in individually ventilated cages under pathogen-free conditions. Animals had free access to food and water and were kept in a 12-hour light-dark cycle.

Preparation of growth factor pellets

Micropellets were prepared in a uniform manner so that they all contain the same amount of the angiogenic or lymphangiogenic stimulus. VEGFA, VEGFC, and control (phosphate-buffered saline, PBS) pellets used for implantation were made with modifications. Pellets contained 10% (w/v) sucralfate (Sigma-Aldrich), 12% (w/v) poly-HEMA (Sigma-Aldrich) dissolved in absolute ethanol, and recombinant human VEGF (VEGF/VEGFA, R&D Systems, Minneapolis MN), VEGFC, or PBS[12]. Pellets were formed by pipetting 5 μl poly-HEMA solution onto UV-exposed parafilm, yielding 20 pellets containing 150 ng VEGFA or VEGFC. Pellets were air dried at room temperature before storage at −80°C. To avoid additional freeze-thaw cycles for the lymphangiogenic factors, which must be stored frozen, the pellets should be carefully stored in small batches. In addition, it is strongly recommended that during preparation, the lymphangiogenic factors are suspended in a low-salt solvent to avoid corneal irritation.

Corneal pellet implantation

A micro pocket for pellet implantation was created. To obtain reproducible results, at least two or more independent experiments were performed. Positive and negative controls were included in each experiment. A carrier molecule such as albumin or a slow-release polymer without an angiogenic or lymphangiogenic factor was used as the negative control.

To obtain statistically meaningful results, we used 5 mice in each group (VEGFA pellet implantation, VEGFC pellet implantation, and control). Phosphate-buffered saline (PBS), in the form of eye drops, was used as a control treatment. *In vivo* imaging was performed on the corneas of the mice at each experimental time point. Upon completion of live imaging, tissues were harvested for postmortem imaging.

Fluorescence microscopy

The transgenic and distinct fluorescence of blood (red) and lymphatic (green) vessels of PGFD mice was observed using a motorized fluorescence stereo zoom microscope (Axio Zoom.V16). This microscope is equipped with a 16x zoom with a high numerical aperture of NA 0.25. It achieves a very high numerical aperture in the medium zoom range with superior fluorescence brightness in large object fields.

Two-photon microscopy

Image acquisition was carried out by a Bruker Pairie Ultima *in vivo* two-photon microscope equipped with an Olympus XLUMPlanFL N 20x/1.00 W objective. EGFP and DsRed were simultaneously excited by a Coherent Chameleon Ultra II two-photon laser tuned to 1000 nm. Emission signals from fluorophores were collected at 520/50 nm (EGFP) and 595/50 nm (DsRed). PrairieView software was used for image acquisition and Imaris (Bitplane, Version 7.2) for image reconstruction.

Quantification of HA and LA in the mouse cornea

Fluorescence images collected using this protocol were compiled, analyzed, and quantified using Adobe Photoshop CS5 image software (Adobe Systems Inc., San Jose, CA). The percentage of the total corneal area that is occupied by blood vessels [(area of blood vessels/total cornea area) × 100] was used as a measurement of corneal HA. The percentage of the total corneal area that is occupied by lymphatic vessels [(area of lymphatic vessels/total cornea area) × 100] was used as a measurement of corneal LA. To quantify changes in corneal HA and LA, measurements taken for each metric at each time point were compared to baseline values.

Results

Imaging of blood and lymphatic vasculature in various tissues/organs of PGFD mice

Based on the transgenic fluorescence of vascular and lymphatic endothelial cells, we applied both confocal and two-photon microscopic imaging to study the patterns of blood and lymphatic vessels in various tissues/organs of the PGFD mouse. We harvested lungs, stomach, skin, heart, intestine, mesentery, and kidney specimens from postnatal day 2. Based on our imaging data, tissues/organs can be divided into two categories: One group with both blood and lymphatic vessels and the other with only blood vessels.

Ear—In PGFD mouse ears we observed that the major branches of blood vessels lie dorsal to the cartilage and are also connected to many small vessels that lie on the ventral surface. Similarly, the network of lymphatic vessels can be seen in green fluorescence where major branches are connected with small subsidiaries (Fig. 1). Another important factor to note is

that in individual images as well as in the merged image, blood vessels are connected at both the ends whereas lymphatic vessels form mostly a blind-ended structure.

Intestine—In the intestine, the main lymphatic branches were visualized at the junction of intestine and mesentery (Fig. 2A) and then radially branched throughout the intestine, forming a network on the intestine wall surface. The blood vessels were found to be more penetrating at the root level than the lymphatic vessels (Fig. 2B). Two-photon microscopic imaging revealed the entire three-dimensional radial network of blood and lymphatic vessels in the intestine (Fig. 2C & D).

Stomach—The blood vessel network was found to be denser in the glandular stomach and the duodenum area than in the forestomach (Fig. 3). Also, the main branches could be seen covering the wall surface, while the small branches ran perpendicular to that of main branches. Similarly, the lymphatic vessel network, although less dense than the blood vessel network, was concentrated more in the glandular stomach. The network of both blood and lymphatic vessels in the ridge area can be seen in the higher magnification image (Fig. 3B). Two-photon microscopic images show the three-dimensional patterns of blood and lymphatic vessels, including lymphatic valves (Fig. 3C).

Lung—The blood and lymphatic vessel networks in the left lobe of the lung were observed by confocal microscopy (Fig. 4). Blood vessels were seen covering the entire wall surface of the left lung lobe while simultaneously running parallel with bronchial tubes to the root. The two dark black holes in the left side of the lung represent the alveolar-spaces (Fig. 4A). The blood vessel network was denser than the lymphatic vessel network. However, the lymphatic vessel network was most dense (bright green) around the upper part of the lobe in the area of lymphoid tissue (Fig. 4A). Two-photon microscopic imaging in the left lung lobe revealed a similar vessel distribution near the alveolar space (Fig. 4C & D).

Kidney and spleen—In PGFD mouse kidneys, we observed blood vessels spread over the fibrous capsule (Fig. 5A). Also, the higher magnification image demonstrates that the blood vessel network penetrated parallel to the renal column, renal medulla surface, and renal pyramid (Fig. 5B). The lymphatic vessel network was not much wider, and a small lumen could only be seen on the wall of the capsule and renal cortex (Fig. 5A & 5B). Two-photon microscopic images show a three-dimensional view of perfusion of the epithelium inside the kidney glomeruli (Fig. 5C). From two-photon microscopic imaging of the spleen (Fig. 5D), it was evident that the major and minor branches of blood vessels are present in both the red and white pulp of the spleen, whereas almost no lymphatic vessels were observed (Fig. 5D).

Skin, mesentery, and heart—In the skin tissue of PGDF mice, the main branches as well as sub-branches of blood vessels ran throughout the tissue, creating vast capillary networks (Fig. 6A & B). Comparatively, the lymphatic vessel network, which mainly consisted of main branches, was observed in the dermis and hypodermal fat layer (Fig. 6A & B). The blood vessels found in the mesentery formed a specific pattern as they all ran parallel to each other and had very few sub-branches, whereas lymphatic vessels followed the blood vessels. A higher magnification image reveals some lymphatic valves (Fig. 6C & D). Two-photon microscopic images show that the blood and lymphatic vessels in the heart

were highly concentrated around the left and right ventricle as opposed to the left and right atrium (Fig. 6E).

Brain—Two-photon microscopic imaging of the brain (Fig. 7A) revealed that the main branches of blood vessels were found in the cerebral cortex and hippocampus and the lymphatic vessel network ran almost parallel to the blood vessels in this section. In the rostral region of the brain near the olfactory bulb, the blood vessel density decreased; however, these vessels were present, which is in contrast to the nearly absent network of lymphatic vessels (Fig. 7B & C). Similarly, imaging of either side of the cerebellum showed a lack of lymphatic vessels but presence of blood vessels (Fig. 7D & E).

Tail, liver and tongue—Blood vessels in the tail were found to form a very dense network throughout the muscle tissue, while also forming some clusters in a repeated pattern as opposed to the lymphatic vessels, which were present in a scattered pattern (Fig. 8A & B). A globular dense pattern of blood and lymphatic vessels was observed throughout the liver globes (Fig. 8C). The blood vessel network was homogenously spread over all papillae in the tongue section (Fig. 8D & E), and some lymphatic valves were present (Fig. 8E).

Live imaging in PGFD mouse corneas

We were able to image both, the growth of individual lymphatic vessels as well as the blood and lymphatic vessel growth pattern following the growth factor implantation in the corneas of live PGFD mice under stereomicroscopy (Fig. 9).

Verification of transgenic fluorescence of blood and lymphatic endothelial cells

To confirm that the endogenous fluorescence observed in the PGFD reporter mice corresponded to Ds-Red and GFP expression by blood and lymphatic endothelial cells, respectively, we performed immunostaining for the different endothelial cells types in harvested corneas. We observed anti-CD31 (PECAM) staining of the blood vessels co-localized in the areas of red fluorescence and LYVE-1 antibody staining co-localized in the areas of green fluorescence (Fig. 10).

HA and LA in the developing mouse cornea

Corneas were harvested from PGFD mice from postnatal day 0 to day 14 or day 60, and the blood and lymphatic vessel networks were observed by confocal microscopy. The blood vessel network is seen to grow on the periphery of limbal and spaced at 90° arc. Lymphatic vessel, following the same pattern shows the maximum growth at Day 6 and Day 10 and then it decreases (Fig. 11).

To investigate the molecular mechanisms of vascular endothelial growth factor receptor 2 (VEGFR2) function in corneal HA and LA, we bred PGFD mice with VEGFR2lox and CDh5CreERT2 mice to generate CDh5CreERT2/VEGFR2lox/PGFD in which membrane-bound (mb)VEGFR2 can be conditionally deleted from vascular endothelial cells. Upon deletion of vascular mbVEGFR2 in tamoxifen-treated CDh5CreERT2VEGFR2lox/PGFD mice, we observed diminished HA and almost no LA after VEGFA pellet implantation (Fig. 13) and almost no LA after VEGFC pellet implantation (Fig. 14).

Discussion

The PGFD transgenic mouse model provides a new platform for simultaneous *in vivo* imaging of injury-induced and growth factor-induced corneal HA and LA progression and regression in the same live mice throughout the course of an experimental study. As the murine and human vasculatures are highly similar, mouse models have been very valuable in studying the progression and regression of blood and lymphatic vessels in various tissues[13]. A major benefit of the new PGFD mice is the ability to image both vessel types in a single mouse at multiple time points. This allows more refined tracking of vascular changes over time, circumvents the effects of between-subject variability, and significantly reduces the number of mice required for *in vivo* experiments. Until now, immunohistochemical staining has been the best available method for simultaneously examining LA and HA *in vivo*[14], newly formed lymphatic and blood vessels could be detected in flattened corneal tissue by staining for the lymphatic endothelial-specific marker LYVE-1 and blood specific marker CD31 respectively. However, the utility of that protocol is limited by the restraints of immunohistochemical staining, most notably the requirement of tissue harvesting (and thus, animal sacrifice). By eliminating the requirements of tissue harvesting and sectioning for antibody staining to visualize vessels, PGFD mice remove the need of sacrificing a mouse for every data point.

The benefit of the inherent transgenic fluorescence of blood and lymphatic vessels in PGFD mice extends beyond the ability for repeated stereomicroscopic *in vivo* imaging in live mice to the ability to use confocal microscopy and two-photon imaging to immediately view three-dimensional blood and lymphatic vessel patterns up to 150 μm and 400 μm deep, respectively, in relatively large and unprocessed specimens of essentially any harvested tissues. This can be applied for analyses of HA and LA at higher magnification upon completion of an experiment involving live *in vivo* imaging of HA and LA in PGFD mouse tissues as well as in studies of the progression, regression, and interaction of blood and lymphatic vessels during development [8] and beyond to the simultaneous observations of HA and LA in any mouse tissue under any variety of experimental conditions. We illustrated this by observing via confocal microscopy imaging the localization of blood and lymphatic vessels in the limbal areas of PGFD mouse eyes harvested at different time points during postnatal development (day 0–adult). Interestingly, we observed enhanced lymphatic vessel growth at postnatal day 6 and peak vessel growth at postnatal day 10, followed by some regression leading to complete lymphatic vessel regression in the adult cornea (Fig. 11) [14,15]. In contrast, no blood vessel growth was observed during the postnatal development of the mouse cornea. We also used confocal microscopy to view the blood and lymphatic vasculature in multiple organs harvested from PGFD mice, including the lung, stomach, skin, heart, intestine, mesentery, and kidney. The PGFD mouse model may be particularly useful for *in vivo* imaging of HA and LA in pathological conditions, such as ischemia and tumor metastasis[16].

In addition to imaging HA and LA in the organs of PGFD mice, we have used these fluorescent reporter mice to characterize corneal HA and LA induced in the normally avascular cornea upon growth factor pellet implantation and corneal alkali burn injury (Fig. 12). The transparent and seemingly delicate anterior surface of the eye has been employed as

an important tool in many major discoveries in the field of HA and, more recently, LA. The cornea is an excellent model for studying the growth of blood and lymphatic vessels for several reasons, including its location on the surface of the animal, where it is easily accessible for experimental manipulation, as well as its inherent avascular nature, which allows observation of vessel formation[17–19]. Corneal neovascularization (CNV), which includes both HA and LA, is a major cause of blindness, and even when corneal transplantation is applied to prevent blindness, CNV greatly increases the risk of transplant rejection [20–22]. While it represents a difficult clinical challenge, CNV also provides a valuable model system for studying the molecular mechanisms of vessel development [15] [17]. Prior research has shown that VEGFA pellet implantation induces both corneal HA and LA, whereas VEGFC pellet implantation induces mainly LA with limited HA [23]. In our experiments, PGFD mouse corneas showed significant progression of HA and LA in response to implantation of pellets of VEGFA and VEGFC growth factors known to trigger the key signaling pathways for HA and LA (Fig. 9). Moreover, by measuring the percentage areas of the cornea covered by blood and lymphatic vessels, we can quantitatively compare HA and LA between different time points and experimental conditions. Overall, observation of the temporal patterns of corneal HA and LA induced by growth factor pellet implantation through *in vivo* live imaging in PGFD mice provides insight into the dynamic trends in pro- and anti-HA and LA factors during these processes.

The dual fluorescence PGFD mice will be valuable for further unraveling the molecular mechanisms of HA and LA through studies involving genetic manipulations, as these processes can be readily observed *in vivo* in corneas of live transgenic knockout mice generated by breeding PGFD mice with other genetically engineered transgenic and knockout mice. VEGFR2 has been shown to play a vital role in HA and LA during normal development, wound healing, and tumor metastasis[16][24–26]. To investigate the molecular mechanisms of VEGFR2 function in corneal HA and LA, we bred PGFD mice with VEGFR2lox mice and then CDh5CreERT2 mice to generate CDh5CreERT2/VEGFR2lox/PGFD mice, in which vascular endothelial cell-derived VEGFR2 can be conditionally deleted. It has been postulated that HA guides LA after injury. However, our observations that deletion of mbVEGFR2 in endothelial cells of blood vessels has differing effects on growth factor-induced HA and LA (Fig. 13 & 14) in the cornea indicate that HA and LA can occur separately[27]. Moreover, consistent with a previous report that HA is negatively controlled by VEGFR-1 acting as a decoy receptor[28] to prevent binding of VEGFA to VEGFR-2[29]. Our observations in PGFD-based conditional knockout mice indicate the important role of vascular endothelial cell-derived VEGFR-2 in the regulation of growth factor-induced LA, and thus, also illustrate the utility of these mouse models for studying the molecular mechanisms of HA and LA in concert[13].

While there are several key advantages to the simultaneous *in vivo* imaging of HA and LA allowed by the PGFD mouse. For all mouse models, these markers allow for targeted imaging of HA and LA, however it is also noticed that Prox1-GFP expression is not exclusively limited to lymphatic endothelial cells [30]. Also, in this model, blood vessels can be visualized generally, but arteries and veins cannot be distinguished using the Flt1-DsRed-based mouse model.

Considering its advantages for many potential uses, the PGFD mouse represents one of the strongest *in vivo* live imaging tools for research into the molecular biology of HA and LA. This newly developed animal model can be used to advance our understanding of the HA and LA processes and their interactions and will hopefully serve as the basis for further advancements in such tools, including *in vivo* and *ex vivo* models for studying HA and LA in health and disease states.

Acknowledgments

This work was supported by grants from the National Institutes of Health [EY10101 (D.T.A.), EY021886, I01 BX002386 (J.H.C), and EY01792 and EY027912 (MIR)], Eversight Midwest Eye Bank Fund (J.H.C) and an unrestricted grant from Research to Prevent Blindness, New York, NY. This work made use of instruments in the Core Imaging Facility (Research Resources Center, UIC)

References

1. Potente M, Makinen T. Vascular heterogeneity and specialization in development and disease. Nature reviews Molecular cell biology advance online publication. 2017; doi: 10.1038/nrm.2017.36
2. Stacker SA, Achen MG, Jussila L, Baldwin ME, Alitalo K. Metastasis: Lymphangiogenesis and cancer metastasis. Nat Rev Cancer. 2002; 2(8):573–583. [PubMed: 12154350]
3. Ohk J, Jung H. Visualization and Quantitative Analysis of Embryonic Angiogenesis in Xenopus tropicalis. Journal of visualized experiments: JoVE. 2017; (123)doi: 10.3791/55652
4. Simons M, Alitalo K, Annex BH, Augustin HG, Beam C, Berk BC, Byzova T, Carmeliet P, Chilian W, Cooke JP, Davis GE, Eichmann A, Iruela-Arispe ML, Keshet E, Sinusas AJ, Ruhrberg C, Woo YJ, Dimmeler S. State-of-the-Art Methods for Evaluation of Angiogenesis and Tissue Vascularization: A Scientific Statement From the American Heart Association. Circ Res. 2015; 116(11):e99–132. DOI: 10.1161/RES.0000000000000054 [PubMed: 25931450]
5. Okabe K, Kobayashi S, Yamada T, Kurihara T, Tai-Nagara I, Miyamoto T, Mukouyama YS, Sato TN, Suda T, Ema M, Kubota Y. Neurons limit angiogenesis by titrating VEGF in retina. Cell. 2014; 159(3):584–596. DOI: 10.1016/j.cell.2014.09.025 [PubMed: 25417109]
6. Kang GJ, Ecoiffier T, Truong T, Yuen D, Li G, Lee N, Zhang L, Chen L. Intravital Imaging Reveals Dynamics of Lymphangiogenesis and Valvulogenesis. Scientific reports. 2016; 6:19459.doi: 10.1038/srep19459 [PubMed: 26785921]
7. Calvo CF, Fontaine RH, Soueid J, Tammela T, Makinen T, Alfaro-Cervello C, Bonnaud F, Miguez A, Benhaim L, Xu Y, Barallobre MJ, Moutkine I, Lyytikka J, Tatlisumak T, Pytowski B, Zalc B, Richardson W, Kessaris N, Garcia-Verdugo JM, Alitalo K, Eichmann A, Thomas JL. Vascular endothelial growth factor receptor 3 directly regulates murine neurogenesis. Genes & development. 2011; 25(8):831–844. DOI: 10.1101/gad.615311 [PubMed: 21498572]
8. Zhu J, Dugas-Ford J, Chang M, Purta P, Han KY, Hong YK, Dickinson ME, Rosenblatt MI, Chang JH, Azar DT. Simultaneous in vivo imaging of blood and lymphatic vessel growth in Prox1-GFP/Flk1::myr-mCherry mice. The FEBS journal. 2015; 282(8):1458–1467. DOI: 10.1111/febs.13234 [PubMed: 25688651]
9. Yang JF, Walia A, Huang YH, Han KY, Rosenblatt MI, Azar DT, Chang JH. Understanding lymphangiogenesis in knockout models, the cornea, and ocular diseases for the development of therapeutic interventions. Survey of ophthalmology. 2016; 61(3):272–296. DOI: 10.1016/j.survophthal.2015.12.004 [PubMed: 26706194]
10. Matsushita J, Inagaki S, Nishie T, Sakasai T, Tanaka J, Watanabe C, Mizutani KI, Miwa Y, Matsumoto K, Takara K, Naito H, Kidoya H, Takakura N, Nagai T, Takahashi S, Ema M. Fluorescence and Bioluminescence Imaging of Angiogenesis in Flk1-Nano-lantern Transgenic Mice. Scientific reports. 2017; 7:46597.doi: 10.1038/srep46597 [PubMed: 28425492]
11. Louveau A, Smirnov I, Keyes TJ, Eccles JD, Rouhani SJ, Peske JD, Derecki NC, Castle D, Mandell JW, Lee KS, Harris TH, Kipnis J. Structural and functional features of central nervous system lymphatic vessels. Nature. 2015; 523(7560):337–341. DOI: 10.1038/nature14432 [PubMed: 26030524]

12. Tang Z, Zhang F, Li Y, Arjunan P, Kumar A, Lee C, Li X. A mouse model of the cornea pocket assay for angiogenesis study. Journal of visualized experiments: JoVE. 2011; (54)doi: 10.3791/3077
13. Chen L, Hann B, Wu L. Experimental Models to Study Lymphatic and Blood Vascular Metastasis. Journal of surgical oncology. 2011; 103(6):475–483. DOI: 10.1002/jso.21794 [PubMed: 21480239]
14. Cao R, Lim S, Ji H, Zhang Y, Yang Y, Honek J, Hedlund EM, Cao Y. Mouse corneal lymphangiogenesis model. Nat Protoc. 2011; 6(6):817–826. DOI: 10.1038/nprot.2011.359 [PubMed: 21637201]
15. Yuen D, Wu X, Kwan AC, Ledue J, Zhang H, Ecoiffier T, Pytowski B, Chen L. Live imaging of newly formed lymphatic vessels in the cornea. Cell research. 2011; 21(12):1745–1749. DOI: 10.1038/cr.2011.178 [PubMed: 22083511]
16. Paduch R. The role of lymphangiogenesis and angiogenesis in tumor metastasis. Cell Oncol (Dordr). 2016; 39(5):397–410. DOI: 10.1007/s13402-016-0281-9 [PubMed: 27126599]
17. Chang JH, Garg NK, Lunde E, Han KY, Jain S, Azar DT. Corneal neovascularization: an anti-VEGF therapy review. Survey of ophthalmology. 2012; 57(5):415–429. DOI: 10.1016/j.survophthal.2012.01.007 [PubMed: 22898649]
18. Chang JH, Gabison EE, Kato T, Azar DT. Corneal neovascularization. Curr Opin Ophthalmol. 2001; 12(4):242–249. [PubMed: 11507336]
19. Walia A, Yang JF, Huang YH, Rosenblatt MI, Chang JH, Azar DT. Endostatin's emerging roles in angiogenesis, lymphangiogenesis, disease, and clinical applications. Biochimica et biophysica acta. 2015; 1850(12):2422–2438. DOI: 10.1016/j.bbagen.2015.09.007 [PubMed: 26367079]
20. Qazi Y, Hamrah P. Corneal Allograft Rejection: Immunopathogenesis to Therapeutics. J Clin Cell Immunol. 2013; 2013(Suppl 9)doi: 10.4172/2155-9899.S9-006
21. Abud TB, Di Zazzo A, Kheirkhah A, Dana R. Systemic Immunomodulatory Strategies in High-risk Corneal Transplantation. J Ophthalmic Vis Res. 2017; 12(1):81–92. DOI: 10.4103/2008-322X.200156 [PubMed: 28299010]
22. Stevenson W, Cheng SF, Dastjerdi MH, Ferrari G, Dana R. Corneal neovascularization and the utility of topical VEGF inhibition: ranibizumab (Lucentis) vs bevacizumab (Avastin). Ocul Surf. 2012; 10(2):67–83. DOI: 10.1016/j.jtos.2012.01.005 [PubMed: 22482468]
23. Cao R, Ji H, Feng N, Zhang Y, Yang X, Andersson P, Sun Y, Tritsaris K, Hansen AJ, Dissing S, Cao Y. Collaborative interplay between FGF-2 and VEGF-C promotes lymphangiogenesis and metastasis. Proceedings of the National Academy of Sciences. 2012; 109(39):15894–15899. DOI: 10.1073/pnas.1208324109
24. Adams RH, Alitalo K. Molecular regulation of angiogenesis and lymphangiogenesis. Nature reviews Molecular cell biology. 2007; 8(6):464–478. [PubMed: 17522591]
25. Albuquerque RJC, Hayashi T, Cho WG, Kleinman ME, Dridi S, Takeda A, Baffi JZ, Yamada K, Kaneko H, Green MG, Chappell J, Wilting J, Weich HA, Yamagami S, Amano S, Mizuki N, Alexander JS, Peterson ML, Brekken RA, Hirashima M, Capoor S, Usui T, Ambati BK, Ambati J. Alternatively spliced vascular endothelial growth factor receptor-2 is an essential endogenous inhibitor of lymphatic vessel growth. Nat Med. 2009; 15(9):1023–1030. doi:http://www.nature.com/nm/journal/v15/n9/suppinfo/nm.2018_S1.html. [PubMed: 19668192]
26. Shibuya M. Vascular endothelial growth factor receptor-1 (VEGFR-1/Flt-1): a dual regulator for angiogenesis. Angiogenesis. 2006; 9(4):225–230. DOI: 10.1007/s10456-006-9055-8 [PubMed: 17109193]
27. Chang LK, Garcia-Cardeña G, Farnebo F, Fannon M, Chen EJ, Butterfield C, Moses MA, Mulligan RC, Folkman J, Kaipainen A. Dose-dependent response of FGF-2 for lymphangiogenesis. Proceedings of the National Academy of Sciences of the United States of America. 2004; 101(32):11658–11663. DOI: 10.1073/pnas.0404272101 [PubMed: 15289610]
28. Simons M, Gordon E, Claesson-Welsh L. Mechanisms and regulation of endothelial VEGF receptor signalling. Nature reviews Molecular cell biology. 2016; 17(10):611–625. DOI: 10.1038/nrm.2016.87 [PubMed: 27461391]

29. Rahimi N, Dayanir V, Lashkari K. Receptor chimeras indicate that the vascular endothelial growth factor receptor-1 (VEGFR-1) modulates mitogenic activity of VEGFR-2 in endothelial cells. J Biol Chem. 2000; 275(22):16986–16992. DOI: 10.1074/jbc.M000528200 [PubMed: 10747927]

30. Choi I, Chung HK, Ramu S, Lee HN, Kim KE, Lee S, Yoo J, Choi D, Lee YS, Aguilar B, Hong YK. Visualization of lymphatic vessels by Prox1-promoter directed GFP reporter in a bacterial artificial chromosome-based transgenic mouse. Blood. 2011; 117(1):362–365. DOI: 10.1182/blood-2010-07-298562 [PubMed: 20962325]

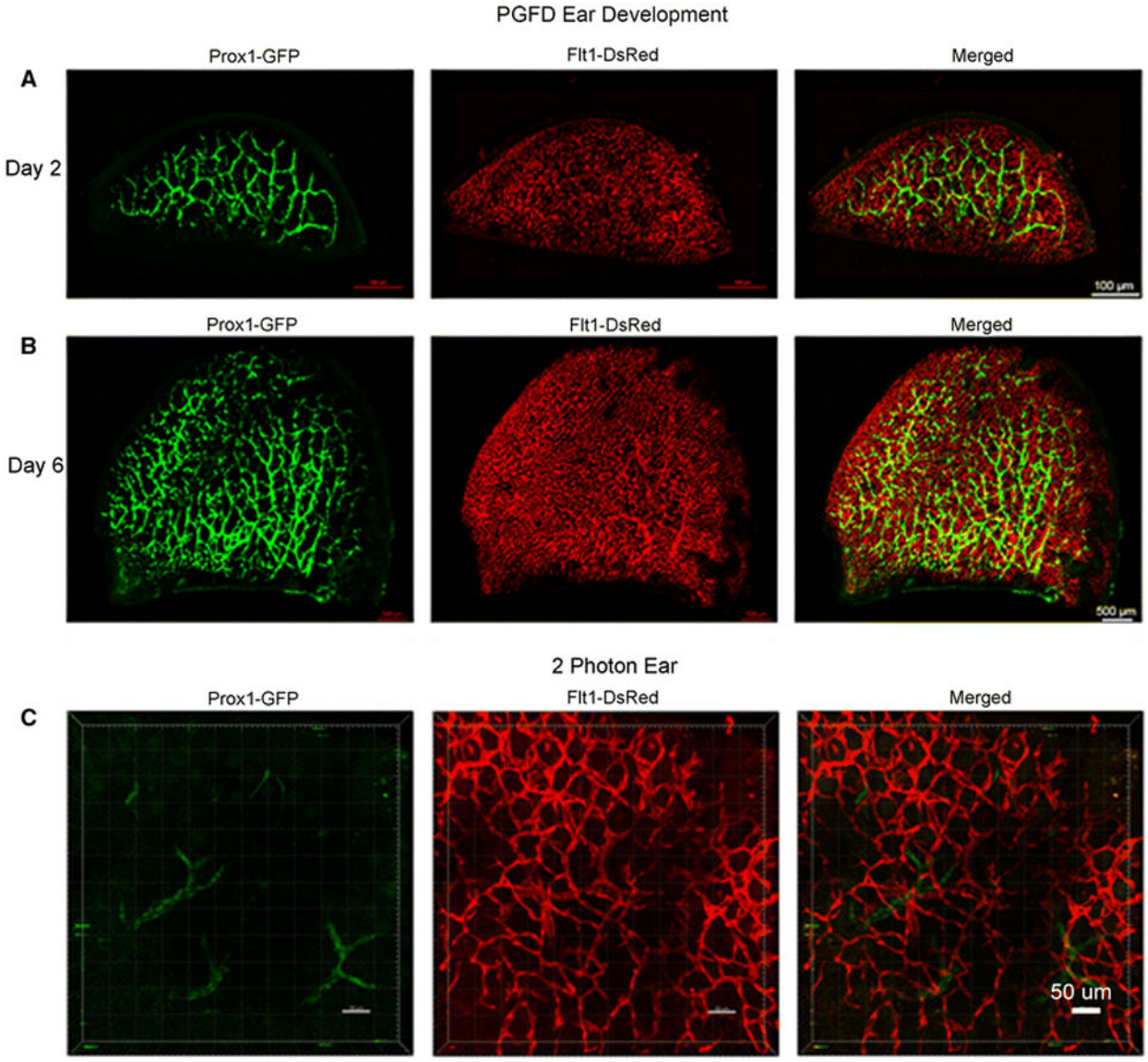

Fig. 1. Confocal microscopy and two-photon images of blood and lymphatic vessels in the PGFD mouse ears

Ears harvested on postnatal days 2 and 6 and from adult mice were imaged using confocal microscopy. Scale bars: (A) 500 μm, (B) 500 μm, and (C) 50 μm.

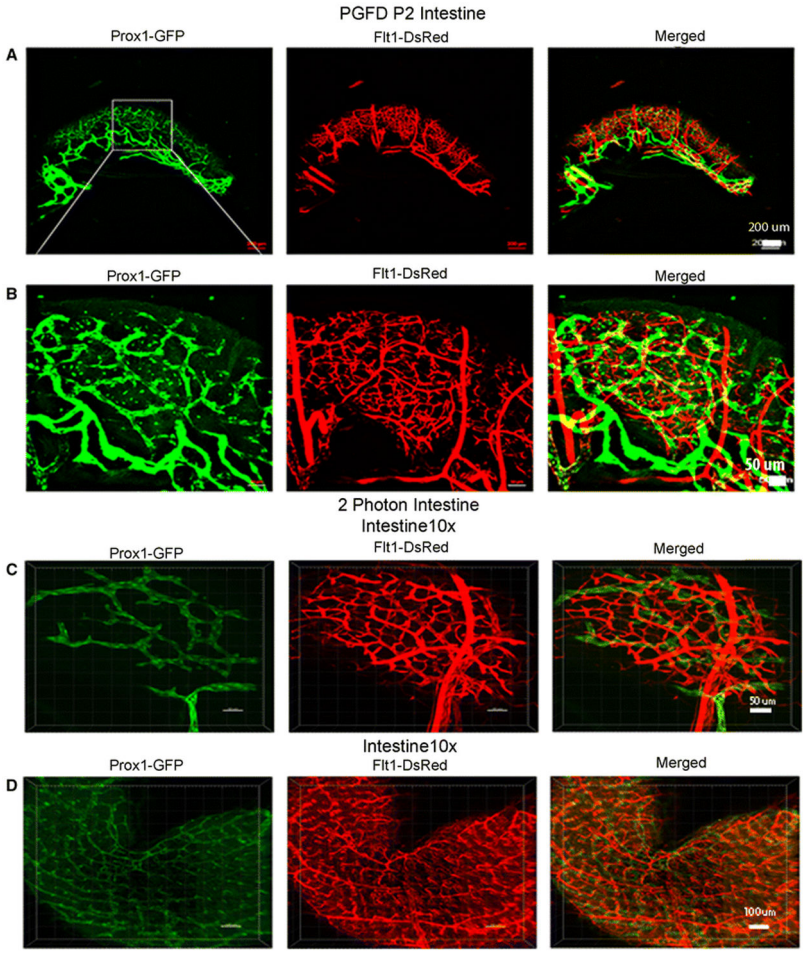

Fig. 2. Confocal microscopy images of blood and lymphatic vessels in the PGFD mouse intestine

(A): Image of blood and lymphatic vessels in PGFD mouse intestines harvested on postnatal day 2. (C & D): Higher magnification images of lymphatic and blood vessels in mouse intestines. Scale bars: (A) 200 μm; (B&C) 50 μm, and (D) 100 μm.

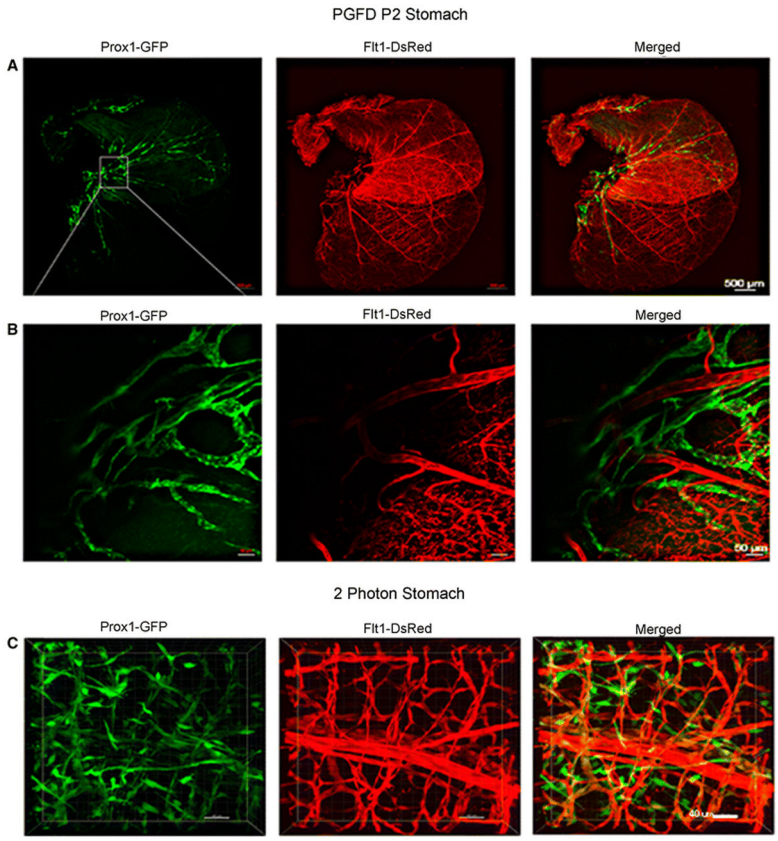

Fig. 3. Confocal microscopy images of blood and lymphatic vessels in the PGFD mouse stomach

(A): Confocal microscopy image of blood and lymphatic vessels in the PGFD mouse stomach harvested on postnatal day 2. (B & C): Higher magnification images of lymphatic and blood vessels. Scale bars: (A) 500 µm; (B) 50 µm; (C) 40 µm.

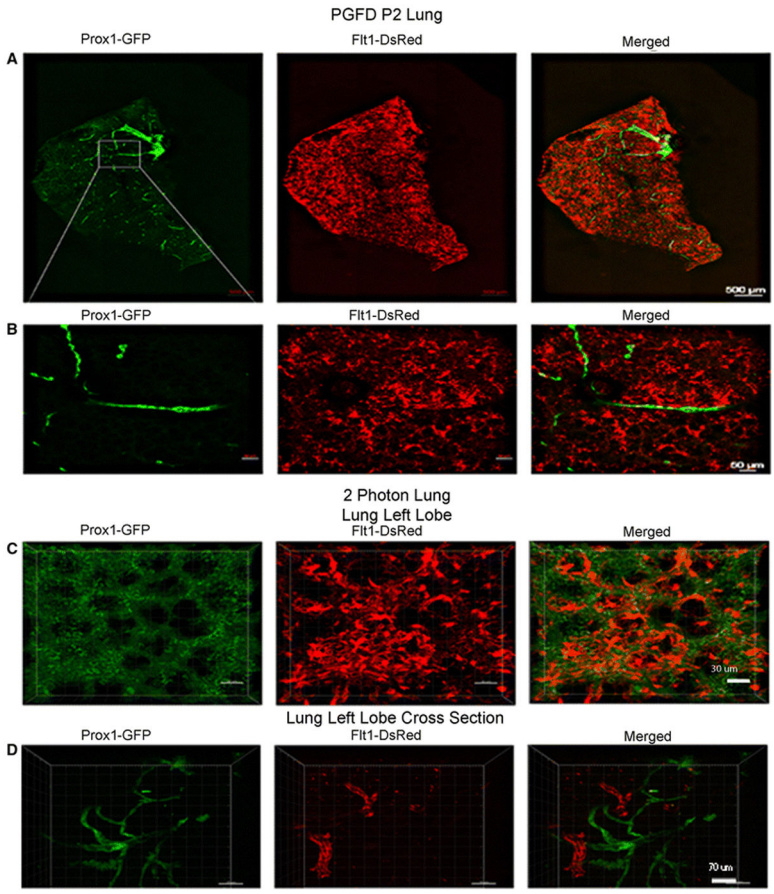

Fig. 4. Confocal microscopy images of blood and lymphatic vessels in the PGFD mouse lung

(A): Confocal microscopy images of blood and lymphatic vessels in the PGFD mouse lung harvested on postnatal day 2. (B, C, D): Higher magnification images of lymphatic and blood vessels. Scale bars: (A) 500 µm; (B) 50 µm; (C) 30 µm, (D) 70 µm.

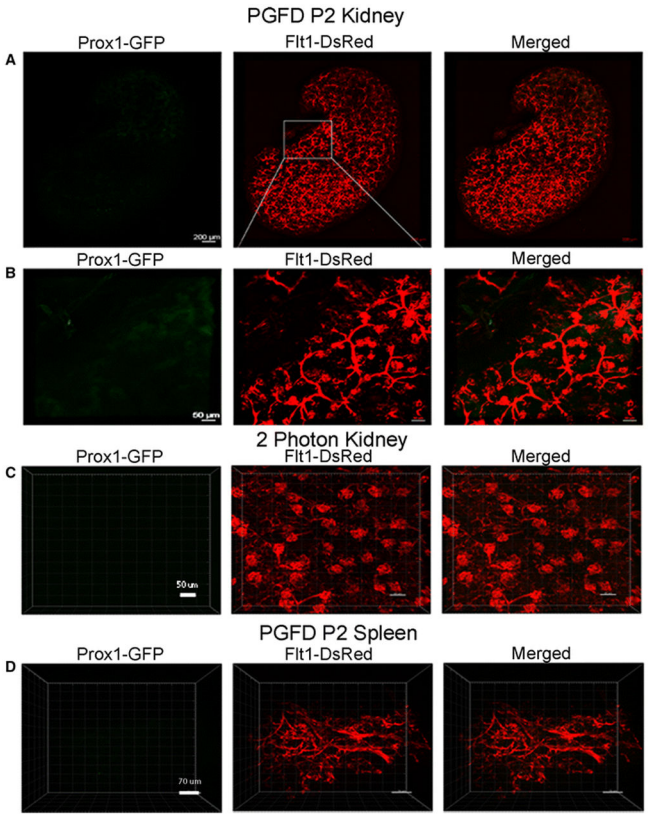

Fig. 5. Confocal microscopy images of blood and lymphatic vessels in the PGFD mouse kidney and spleen

(A): Confocal microscopy image of blood and lymphatic vessels in the PGFD mouse kidney harvested on postnatal day 2. (B & C): Higher magnification images of lymphatic and blood vessels. (D): Confocal microscopy image of blood and lymphatic vessels in the PGFD mouse spleen harvested on postnatal day 2. Scale bars: (A) 200 μm; (B) 50 μm; (C) 50 μm, (D) 30 μm.

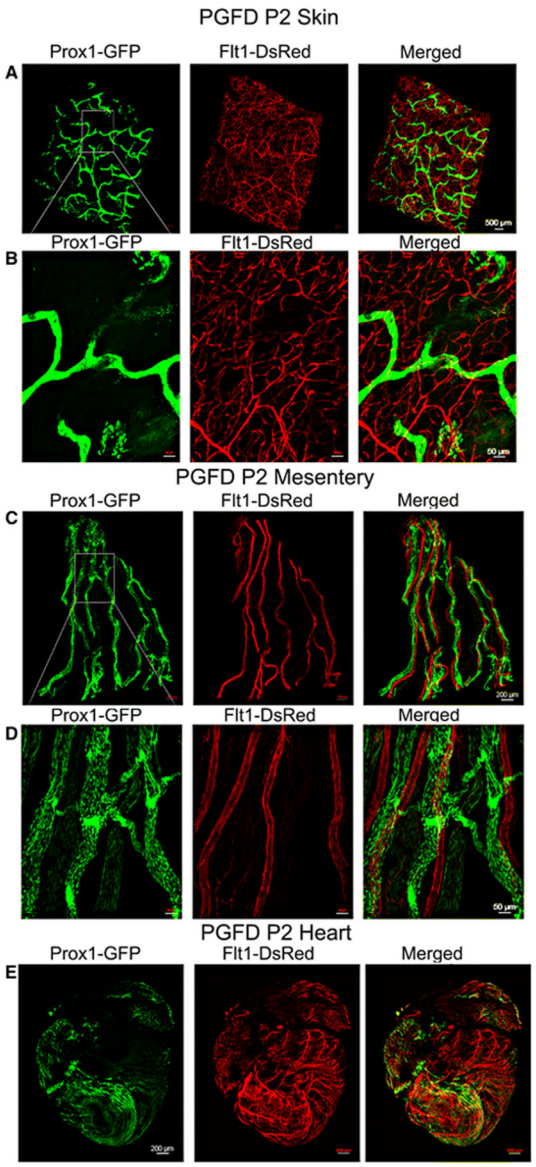

Fig. 6. Confocal microscopy images of blood and lymphatic vessels in the skin, mesentery and heart of the PGFD mouse

(A): Confocal microscopy image of blood and lymphatic vessels in the PGFD mouse skin harvested on postnatal day 2. (B): Higher magnification image of lymphatic and blood vessels. Scale bars: (A) 500 μm; (B) 50 μm.

(C): Confocal microscopy image of blood and lymphatic vessels in the PGFD mouse mesentery harvested on postnatal day 2. (D): Higher magnification image of lymphatic and blood vessels. Scale bars: (C) 200 μm; (D) 50 μm.

(E): Confocal microscopy image of blood and lymphatic vessels in the PGFD mouse heart harvested on postnatal day 2. Scale bar (E) 200 μm.

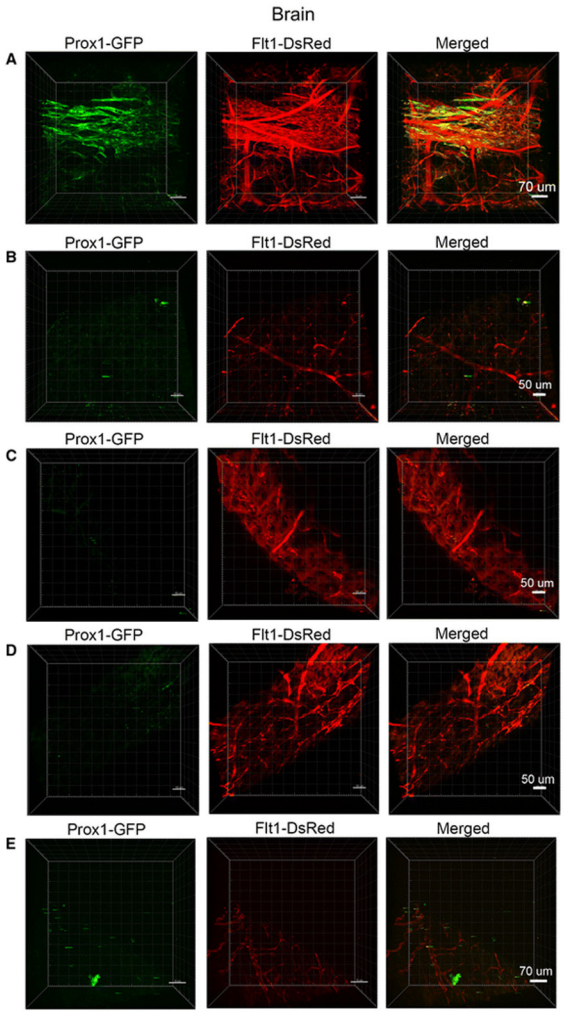

Fig. 7. Confocal microscopy images of blood and lymphatic vessels in the PGFD mouse brain

(A): Confocal microscopy image of blood and lymphatic vessels in the PGFD mouse brain harvested on postnatal day 2. (B, C, D, E): Higher magnification images of lymphatic and blood vessels. Scale bars: (A) 70 μm; (B) 50 μm (C) 50 μm (D) 50 μm; (E) 70 μm.

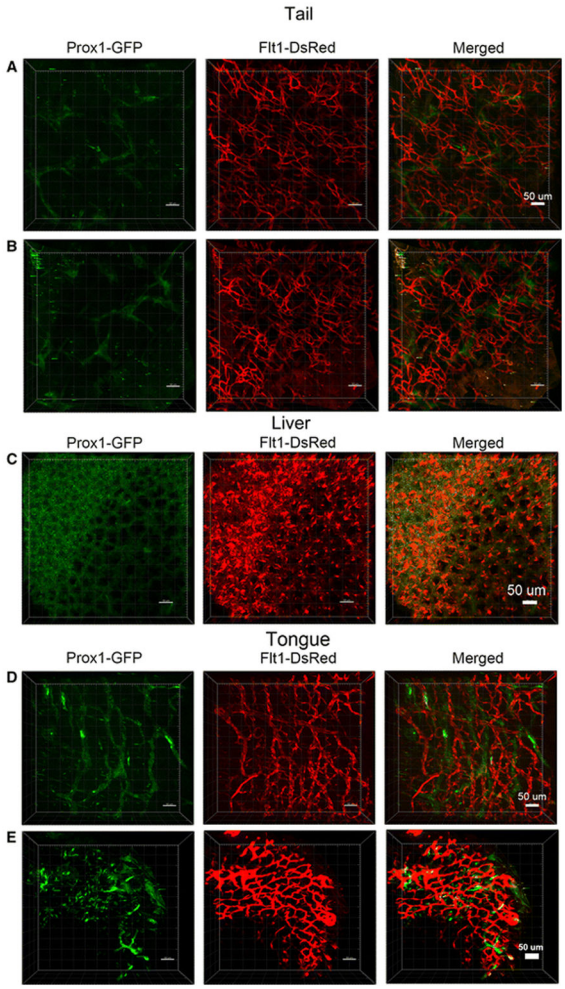

Fig. 8. Confocal microscopy images of blood and lymphatic vessels in the tail, liver and tongue of the PGFD mouse

(A): Confocal microscopy image of blood and lymphatic vessels in the PGFD mouse tail harvested on postnatal day 2. (B): Higher magnification image of lymphatic and blood vessels. Scale bars: (A) 50 μm; (B) 50 μm. (C): Confocal microscopy image of blood and lymphatic vessels in the PGFD mouse liver harvested on postnatal day 2. Scale bar: (C) 50 μm. (D): Confocal microscopy image of blood and lymphatic vessels in the PGFD mouse tongue harvested on postnatal day 2. (E): Higher magnification image of lymphatic and blood vessels. Scale bars: (D) 50 μm; (E) 50 μm.

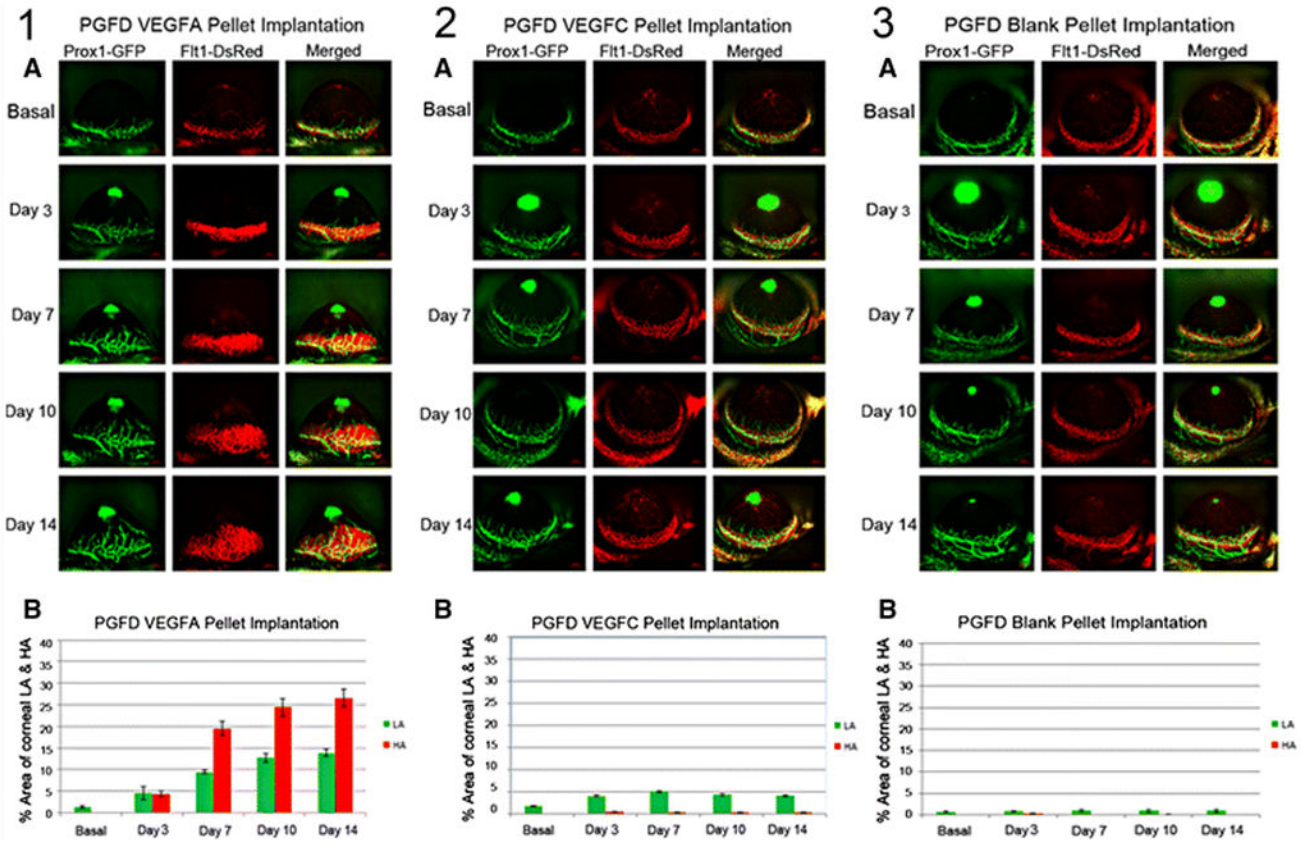

Fig. 9. VEGFA– and VEGFC–induced corneal LA and HA in PGFD mice

Axiozoom stereo microscopy was used to image the vascular (red) and lymphatic (green) vessels within the same cornea at each time point. (1A) After VEGFA corneal pellet implantation, enhanced corneal LA and HA were observed on days 3, 7, 10 and 14. (1B) The percent area occupied by VEGFA–induced corneal LA and HA was followed over the experimental time course and increased significantly by day 7 (days 7, 10 and 14 vs. basal). (2A) After VEGFC corneal pellet implantation, enhanced corneal LA was observed on days 3, 7, 10, and 14, and the areas of corneal VEGFC–induced LA increased significantly on days 3, 7, 10 and 14 (vs. basal). (2B) The percent area occupied by VEGFC–induced corneal LA was followed over the experimental time course. (3A) After blank pellet implantation, no induction of corneal HA and LA were observed on days 3, 7, 10, and 14. (3B) The percent area occupied by PBS-induced corneal LA was calculated over the experimental time course.

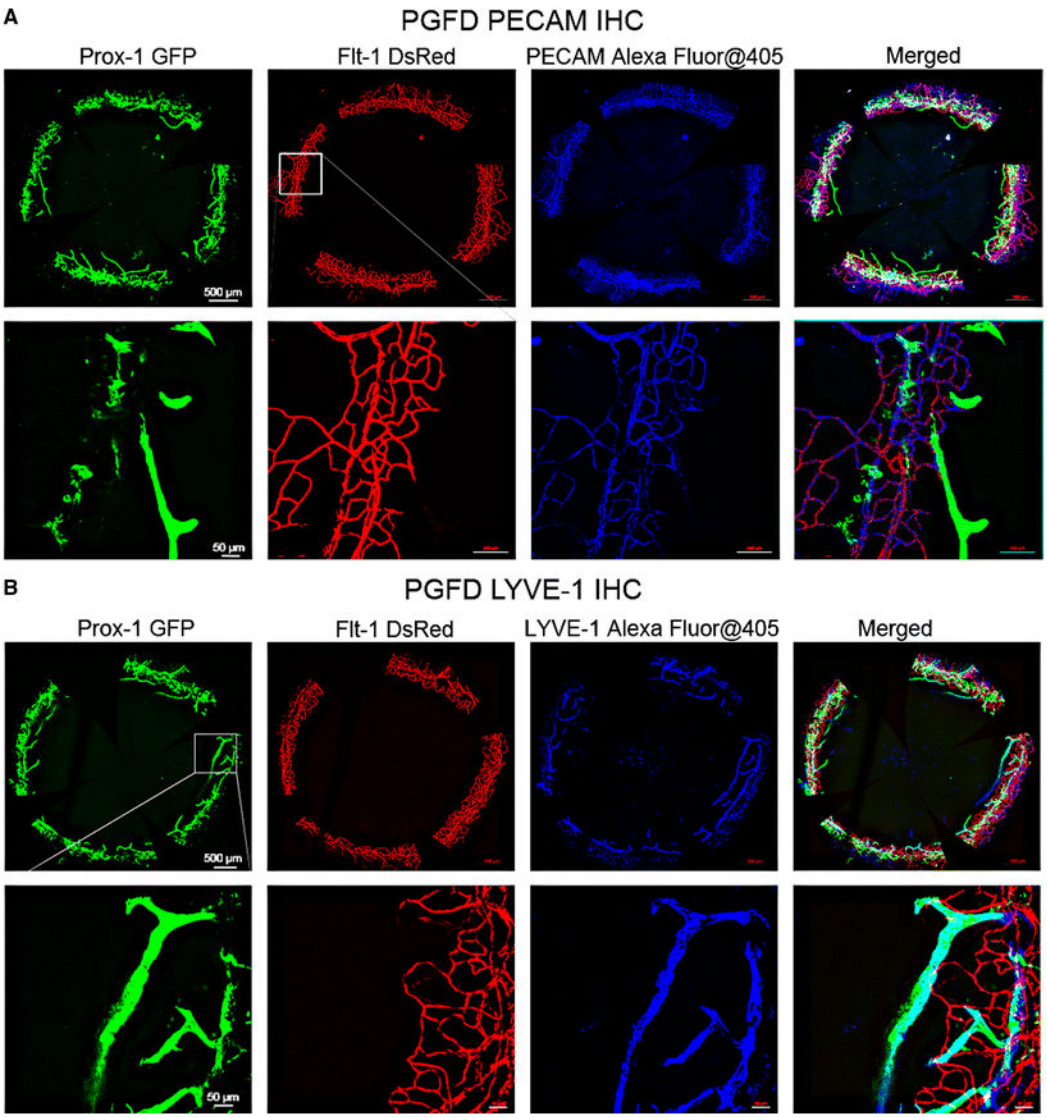

Fig. 10. Immunostaining of blood and lymphatic vessels in whole-mount corneas from PGFD mouse

PGFD mouse corneas were immunostained with anti-PECAM-1 antibody (A, blue imaging) and anti-LYVE-1 antibody (B, blue imaging). DsRed-expressing vessels co-localized with PECAM-1–immunostained blood vessels and GFP-expressing vessels co-localized with LYVE-1–immunostained lymphatic vessels were visualized. Scale bars: top row, 500 μm;bottom row, 50 μm.

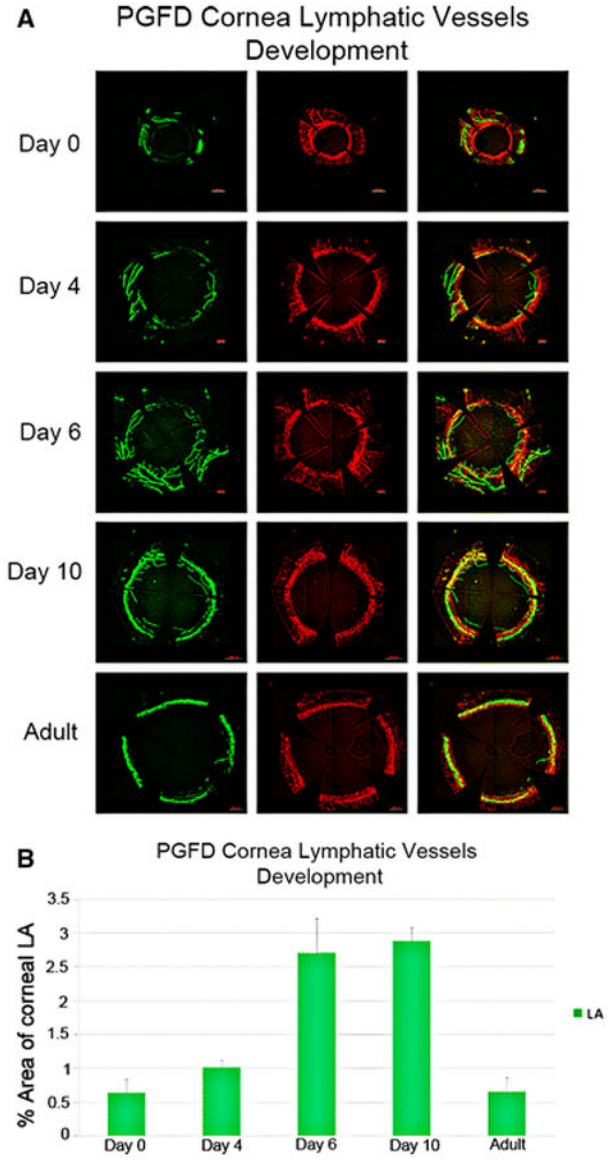

Fig. 11. Spontaneous corneal LA during postnatal corneal development in PGFD mice

(A) Confocal microscopy images of blood and lymphatic vessels in PGDF mouse corneas harvested on postnatal days 0, 4, 6, and 10 and from an adult mouse. (B) Percent area covered by lymphatic vessels in postnatal corneas. Blood and lymphatic vessels were localized to the limbal area on postnatal day 0. Lymphatic vessel growth was enhanced on day 6; peak vessel growth was observed on day 10 and the vessels had completely regressed in the corneas that were later obtained from adult mice. No blood vessel growth in the corneas was observed during postnatal development.

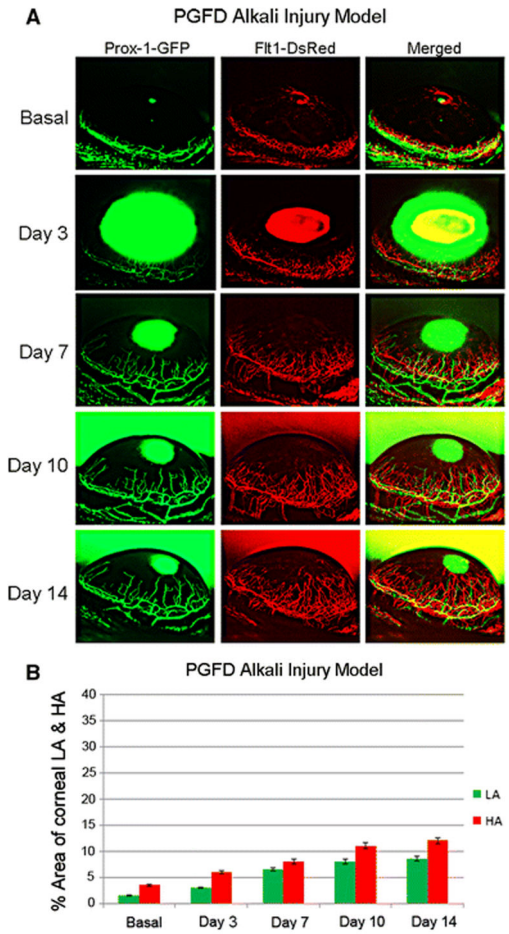

Fig. 12. Alkali burn–induced corneal HA and LA in PGFD mice

Axiozoom stereo microscopy was used to image the vascular (red) and lymphatic (green) vessels within the same cornea at each time point. (A) Blood and lymphatic vessel growth were quantitatively compared according to the percent area of the cornea that was occupied by each vessel type. (B) The percent area occupied by alkali burn–induced corneal HA and LA was calculated over the experimental time course.

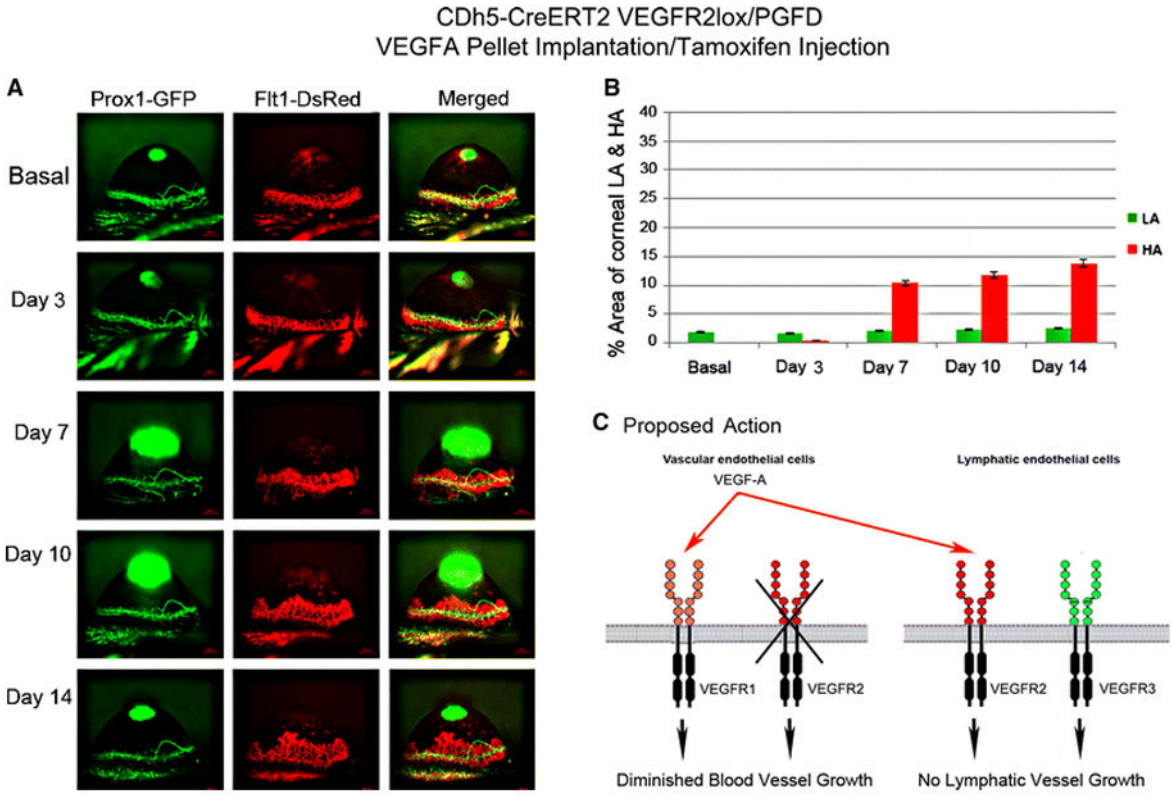

Fig. 13. VEGFA–induced corneal HA and LA in tamoxifen-treated CDh5CreERT2/VEGRF2lox/PGFD mice

Axiozoom stereo microscopy was used to image the vascular (red) and lymphatic (green) vessels within the same cornea at each time point. (1A) Eliminated corneal LA and significantly increased HA in VEGFR2 knockout in vascular endothelial cells were observed on days 7, 10, and 14 after 150 ng VEGFA corneal implantation when compared to that observed in the tamoxifen-treated CDh5-CreERT2VEGRF2lox/PGFD mice. (1B) The percent area occupied by VEGFA–induced corneal HA and LA was calculated over the experimental time course.

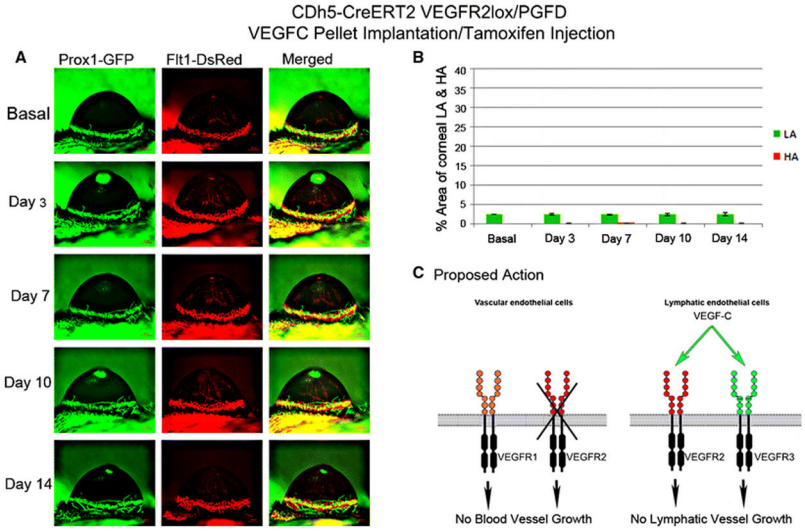

Fig. 14. VEGFC–induced corneal HA and LA in tamoxifen-treated CDh5CreERT2/VEGRF2lox/PGFD mice

Axiozoom stereo microscopy was used to image the vascular (red) and lymphatic (green) vessels within the same cornea at each time point. (2A) No VEGFC–induced corneal LA was observed in tamoxifen-treated CDh5-CreERT2 VEGFR2lox/PGFD mice after implantation of a 150 ng VEGFC pellet. (2B) The percent area occupied by VEGFC–induced corneal LA was followed over the experimental time course.